photonics

MDPI

Article

Effect of Plasmonic Au and Ag/Au Nanoparticles and Sodium Citrate on the Optical Properties of Chitin-Based Photonic Nanoarchitectures in Butterfly Wing Scales

Krisztián Kertész *, Gábor Piszter, Zsolt Endre Horváth, Dániel Zámbó, András Deák and László Péter Biró

Centre for Energy Research, Institute of Technical Physics and Materials Science, 29-33 Konkoly-Thege Miklós Street, 1121 Budapest, Hungary
* Correspondence: kertesz.krisztian@ek-cer.hu

Abstract: Porous butterfly wings with hierarchically organized structures from nanometer to centimeter scales were tested as substrates for carrying plasmonic Au and Ag/Au nanoparticles with potential application in photocatalysis. Wings exhibiting structural color generated by chitin-air nanocomposites were used. Hundreds of butterfly species possess these types of color-generating photonic nanoarchitectures, producing color by a similar mechanism to manmade photonic crystals. Artificial photonic crystals are known to enhance photocatalytic processes through the slow light effect. The impact of pure water, water-based sodium citrate solution, and Au and Ag/Au alloy nanoparticles on the optical properties of the natural photonic structures were separated. While water and aqueous sodium citrate solutions change the wing reflectance by the alteration of the wing scale position with respect to the wing plane, Au and Ag/Au alloy nanoparticles form a new, hybrid nanostructure with the chitin nanoarchitecture modifying the structural color of the butterfly wings. The optical properties of the new types of hybrid photonic nanoarchitectures (consisting of butterfly wings and plasmonic nanoparticles) are different from those of the components.

Keywords: photonic crystal; butterfly wing; plasmonic metallic nanoparticle; sodium citrate; water

Citation: Kertész, K.; Piszter, G.; Horváth, Z.E.; Zámbó, D.; Deák, A.; Biró, L.P. Effect of Plasmonic Au and Ag/Au Nanoparticles and Sodium Citrate on the Optical Properties of Chitin-Based Photonic Nanoarchitectures in Butterfly Wing Scales. *Photonics* **2022**, *9*, 553. https://doi.org/10.3390/photonics9080553

Received: 22 June 2022
Accepted: 2 August 2022
Published: 6 August 2022

1. Introduction

Photocatalysis based on optically activated, plasmonic metal nanoparticles (NP) has emerged as a promising approach to facilitate light-driven chemical conversions under far milder conditions than thermal catalysis [1]. This field of heterogeneous catalysis, known as plasmonic photocatalysis, exploits visible-light-driven chemical transformations on plasmonic metal nanostructures [2]. For example, in the case of Au NPs, the light-driven excitation shows both plasmonic and interband effects [3]. A very important advantage of such catalytic reactions is the possibility of using solar radiation to carry out, for example, water quality improvement with low energy input and in an environmentally friendly way [4–6]. Photocatalysis on non-toxic, stable metallic NPs such as Au or Ag/Au alloys, which offer the possibility to tune the wavelength range where photoexcitation is occurring, is ideal to be used for clean and safe technology [2]. To be able to exploit this advantage, the metallic NPs must be supported on a substrate [7,8] which will provide a large specific surface area, possibly by micro- and nanostructuring, and can be produced in a cheap and environmentally friendly way.

Photonic-crystal-type (PhC) structures, in particular, inverse opal type nanoarchitectures, are used to host various catalytic NPs [9]. Moreover, near IR to UV upconversion has been demonstrated with core–shell NPs in PhCs [10]. Slow light effects [11] and strong vibrational coupling of molecules inside a cavity [12,13] have much potential for molecular and material sciences that is just beginning to be explored. So, these hybrid nanoarchitectures (PhC + NP) exhibit a lot of potential for harnessing solar radiation for catalytic purposes. Unfortunately, the fabrication of large areas and good quality three-dimensional

(3D) PhCs is still very challenging [14]. On the other hand, as many studies reported, a rich "library" of PhC-type nanoarchitectures of biologic origin can be found on the wings of butterflies exhibiting structural coloration [15–21]. The photonic nanoarchitectures of butterflies exhibit excellent stability over time (for periods exceeding 100 years) [22]; for certain species, only moderate variability [23] is shown because these colors are most frequently used in the sexual communication of butterflies and exhibit only moderate variation on a continental scale [24].

The simplest way of producing nanocomposites of metallic NPs in PhC-type nanoarchitectures in butterfly wing scales is the application of colloidal sols of metallic NPs on the flat butterfly wing. In this process, the effect of three major sol components has to be taken into account: the effect of water, the metallic Au and Ag/Au alloy NPs, and the sodium citrate used for the formation/stabilization of the NPs [25–27]. In the present paper, the impact of these three components on the optical properties of the natural photonic nanoarchitectures is discussed.

At first glance, it may seem both impractical and questionable from an environmental conservation point of view to use butterfly wings as components of hybrid photocatalytic nanocomposites. However, a more thorough examination of this question will hopefully eliminate these concerns. The world production of natural silk is based on the cocoons of the domesticated mulberry moth (*Bombyx mori*) and amounts to about 80,000 tons/year [28], dating back more than 1000 years [29]. In a dedicated insectarium (Figure S1), it was possible to obtain more than 600 *Polyommatus icarus* exemplars from a single breeding pair, so if the need arises, it may be possible to produce a large number of butterfly wings without endangering wildlife conservation.

2. Materials and Methods

The blue wings of male *P. icarus* butterflies obtained in a laboratory breeding experiment were used in the present study. All used specimens were descendants of the same breeding pair. The butterflies were collected immediately after they extended and dried their wings and were killed by freezing without the use of any chemicals. The blue color of the males is produced by a so-called "pepper-pot"-type, quasiordered photonic nanoarchitecture [16]. The reflectance maximum of the nanoarchitectures producing the structural color is fairly stable, even after on-purpose alteration of the developmental cycle of the butterflies [30].

The Au NP sol was produced by the citrate-assisted Turkevich method in an aqueous medium [31]. Briefly, $HAuCl_4 \cdot 3H_2O$ solution (0.01 M, 6 mL) was mixed with ultrapure water (222 mL) in a 500 mL reaction bottle. The solution was brought to a boil under continuous stirring, and when the boiling started, sodium citrate trihydrate solution (0.0684 g in 6 mL) was swiftly injected. The solution was boiled for 15 min whilst the particles formed, and the solution turned ruby red. Afterwards, the gold NP solution was allowed to cool to room temperature. The extinction spectrum of the as-synthesized particles is shown in Figure S2. The particles have an LSPR peak position at 516 nm and have an average hydrodynamic diameter of 18 nm.

The bimetallic sol of alloyed Ag/Au NPs of Ag/Au = 1/1 atomic ratio was produced according to the preparation method reported in ref. [32]. Two aqueous solutions of 50 mL containing 0.01 mmol $HAuCl_4$ and 0.01 mmol $AgNO_3$ (both from Sigma-Aldrich (Burlington, MA, USA)), respectively, besides 0.05 mmol sodium citrate, were preheated under stirring up to boiling, mixed together and continuously stirred under reflux for 30 min, then under cooling to room temperature. The visible absorbance spectrum of the resulting sol is presented in Figure S3. The average size of the alloyed Ag/Au nanoparticles was determined using transmission electron microscopy, and an average diameter of 23 nm was found.

Two different sodium citrate solutions were used: (a) obtained by the centrifugation (using 1 mL solution at 9000 rcf, 30 min) of the sol of Au and using the clear supernatant, (b) 1.0 M aqueous sodium citrate solution as a blank of the Ag/Au sol.

As the butterfly wings are superhydrophobic [33], to facilitate wetting with water-based solutions, a drop of ethanol was used to wet the wings before the drop-drying of the Au or Ag/Au sols. From here on, this procedure will be called soaking.

In some experiments, PTFE frames were used. These were prepared by cutting using a blade from 2 mm thick plates purchased from Sigma-Aldrich (Burlington, MA, USA).

In order to add mechanical stability, the wings were mounted on microscope glass slides by gluing with melted polylactic acid (PLA).

As a reference sample without photonic nanoarchitecture, filter paper was used in the form of cutting 1 cm^2 pieces from the VWR filter disk (type 424). Filter paper loading by magnetic stirring was carried out using a Heidolph MR 3001 magnetic stirrer by immersing the filter paper in the stirred sol.

Chitin powder was purchased from Sigma-Aldrich (Burlington, MA, USA).

Reflectance spectroscopy measurements were conducted using an Avantes (Apeldoorn, The Netherlands) fiber-optic system consisting of an AvaSpec-HERO spectrometer, an AvaLight-DH-S-BAL stabilized UV-visible light source, an AvaSphere-30-REFL integrating sphere, and a bifurcated reflectance probe (FCR-7UV200-ME-SR). For both normal incidence and integrating sphere measurement modes, a WS-2 white diffuse tile was used as a reference.

Microspectrometric measurements on single scales removed from the wing were carried out using a Zeiss Axio Imager A1 (Jena, Germany) optical microscope supplemented with a custom-made adapter tube which connected the Avantes spectrometer to the $\times 50$ Epiplan objective.

Focus stacking microscope measurements were carried out using a Nikon (Nikon Instruments, Tokyo, Japan) Eclipse LV150N device with a $\times 50$ objective and extended depth of focus (EDF) mode; supplemented with a calibrated motorized stage, we were able to conduct height measurements of cover scale rows.

3. Results

The first question to be answered for the present work concerns the interaction of liquid water with the butterfly wing. To answer this, the butterfly wings were mounted on a glass substrate and immersed in deionized water for 6 days without any other pretreatment. In Figure 1, the wings' status before immersion and at the end of the immersion period is shown. The normal incidence reflectance spectra of the immersed wings were measured after 72 h of immersion, immediately after their removal from water and in the following 8 h (Figure 2). A slight redshift can be observed in the measured structural color. One may note that in the first hour of drying, the redshift in the spectral position of the reflectance maximum is eliminated, and the coloration remained constant in the following hours, both in amplitude and the spectral position of the reflectance maximum.

In the next step, 40 µL of sodium citrate-based Au NP sol was drop-dried on both the fore and the hindwing of the same butterfly specimen. The samples were measured before drop-drying and after complete drying. The normal incidence reflectance of the wings measured before drop-drying and after complete drying is shown in Figure 3a. In order to clarify the origin of the significant increase (of the order of 40%) in the reflectivity of the samples, the same wings were also measured with an integrating sphere, both before and after drop-drying. The resulting spectra shown in Figure 3b also exhibit some increase in reflectivity (about 5%), but far less than the spectra measured in normal incidence. Both in the normal incidence and the integrating sphere measurements, a slight redshift in the spectral position of the reflectance maximum is present after drying.

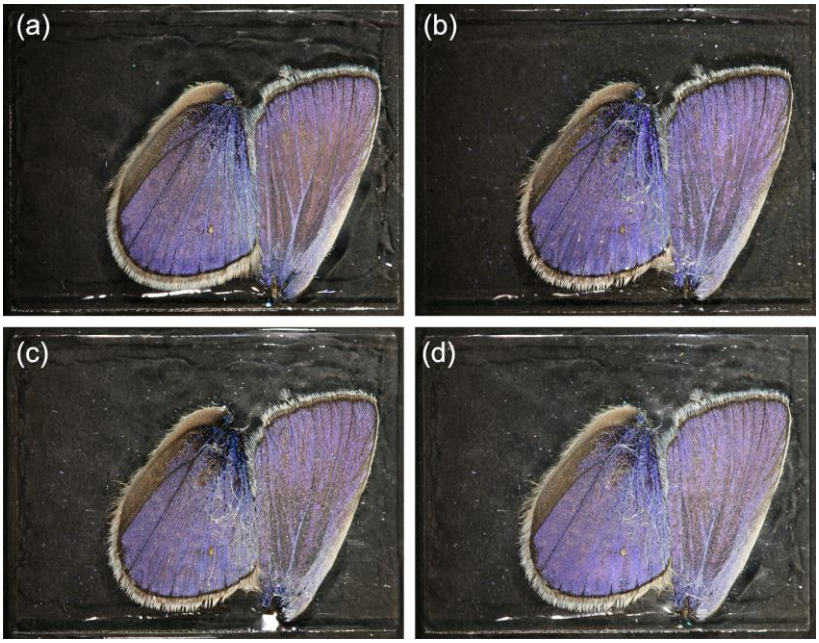

Figure 1. The *Polyommatus icarus* wings mounted on glass slides after 6 days of immersion in water (in horizontal position) did not lose structural color but suffered some redshift, indicating a moderate swelling of the chitin nanoarchitecture. (**a**) Pristine dry wings; (**b**) wings immediately after immersion; (**c**) wings after 6 days of immersion, removed from water; (**d**) wings 5 h after removing from water.

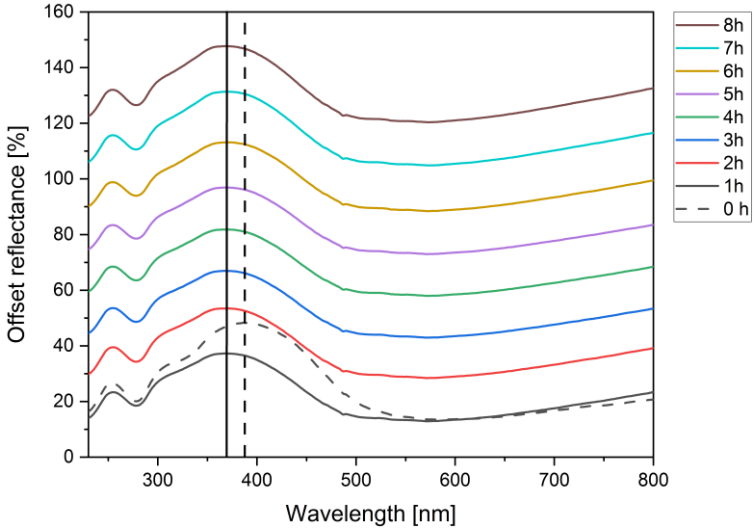

Figure 2. Normal incidence reflectance spectra of a blue *Polyommatus icarus* wing in air after 72 h of immersion in deionized water (dashed curve) and during the following eight hours. The spectra of the drying wing taken at one-hour intervals were offset vertically to enhance clarity. After the first hour of drying, no significant changes occurred.

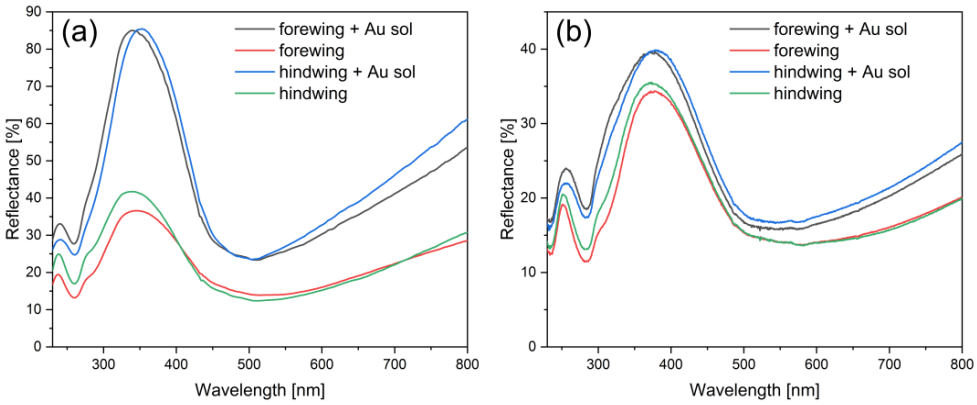

Figure 3. Reflectance measured on the wings of a male *Polyommatus icarus* butterfly before and after the drop-drying of sodium citrate-based Au NP sol. (**a**) Measurement in normal incidence: red and green curves show the pristine status, and the black and blue curves were taken after the complete drying; (**b**) measurement with an integrating sphere: red and green curves show the pristine status, and the black and blue curves were taken after the complete drying.

Next, using the integrating sphere setup, the effect of the amount of the applied NP sol was tested by drop-drying increasing amounts of sol, as shown in Figure 4. To avoid the uncontrolled spreading of the larger amount of liquid, e.g., when 120 µL of sol was applied, the wings were sandwiched between a glass slide and a PTFE frame, as seen in Figure 4a. Wings with a similar spectral position of the pristine reflectance maximum were used (Figure S4). One may note that the three times increase in the amount of the applied sol produced a more pronounced redshift of the reflectance maximum, but the increase of the amplitude of the maximum stayed in the range of 5%, as in Figure 3b. When examining the dried wing by SEM, one may clearly observe the presence of Au NPs on the chitinous nanostructure (Figure 5).

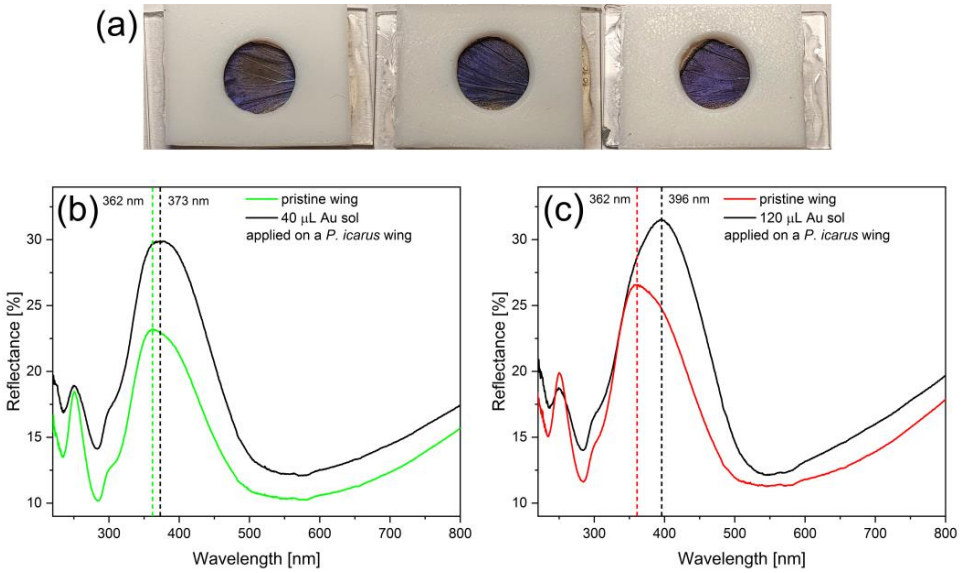

Figure 4. (**a**) Photographs of the butterfly wings in the PTFE frames used for the measurements; (**b**) Integrating sphere reflectance measurements in pristine state before the application of the NP sol and after the application of 40 µL of Au sol and complete drying; (**c**) integrating sphere reflectance measurements in pristine state before the application of the sol and after the application of 120 µL of Au sol and complete drying.

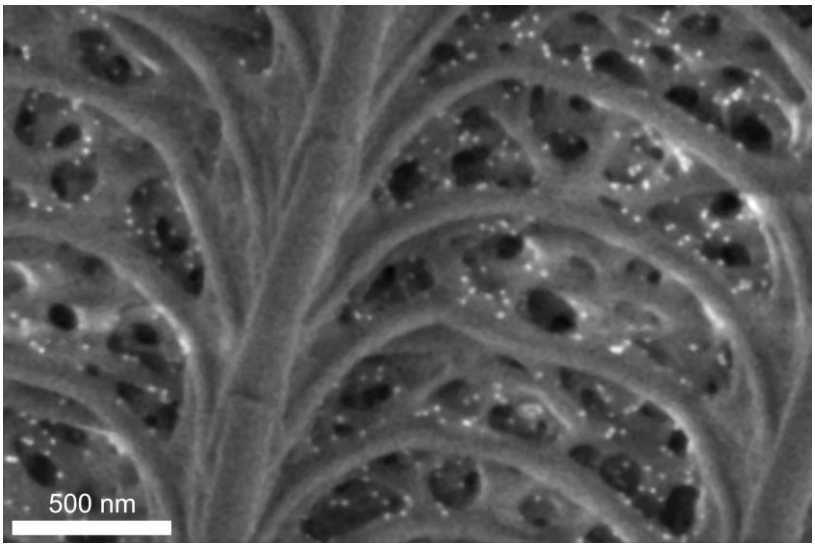

Figure 5. Scanning electron micrograph of a scale of the *Polyommatus icarus* wing after the application of 120 µL of Au NP sol and complete drying. One may note the presence of bright dots in the image, which represent the Au NPs.

The thickness of the PTFE frame did not allow close contact between the butterfly wing and the illumination port of the integrating sphere; therefore, in the subsequent experiments, butterfly wings were mounted directly on the glass substrate and only PLA gluing was used. A total of 40 samples were prepared and subjected to different treatments. The results following the statistical evaluation are summarized in Figure 6. One may observe that PLA gluing produced a slight blueshift in the spectral position of the reflectance maximum (Figure 6a), but on average, the amplitude of the reflectance maximum in normal incidence did not change significantly (Figure 6b). The subsequent water immersion for 8 h, followed by overnight drying, did not produce modifications of the spectral position and the amplitude of the reflectance maximum. The drop-drying of sodium citrate solution returned the spectral position of the reflectance maximum to that of the pristine state (redshift) but produced a significant increase in the amplitude of the normal incidence reflectance. The removal of the dried citrate by immersing the samples for 8 h in water and measuring them after overnight drying in air eliminated the redshift in the spectral position but preserved the increased amplitude of the reflectance maximum.

When not only pure sodium citrate solution but Au NP sol in citrate solution was applied on the water-immersed and dried butterfly wings, the observed effects presented the characteristics of the citrate solution application, but an additional redshift was produced (Figure 6a), and the increase in the amplitude of the normal incidence reflectance maximum was slightly smaller (Figure 6b).

The statistical data in Figure 6 are in good agreement with the data obtained on individual wings, presented in Figures 3 and 4.

In the next experiment, Au and alloyed Ag/Au NPs were used as the extinction peaks of the two different kinds of NPs have different spectral positions (Figures S2 and S3). Additionally, white filter paper was used as a comparison sample with filamentous structure because the chemical composition of cellulose, the major component of the paper, is also a polysaccharide with very close chemical properties to that of chitin [34].

In Figure 7a, the reflectance of the pristine filter paper is compared with the reflectance of the filter paper loaded with Ag/Au NPs by immersion in stirred Ag/Au sol. In Figure 7b, the samples resulting from the same filter paper are shown after loading with Au and Ag/Au NPs, respectively. The same amount of the two NP sols was used. It can be clearly seen that the absorption of the Ag/Au NPs is positioned on the blue side of the absorption of the Au NPs (centered at 473 nm and 520 nm, respectively).

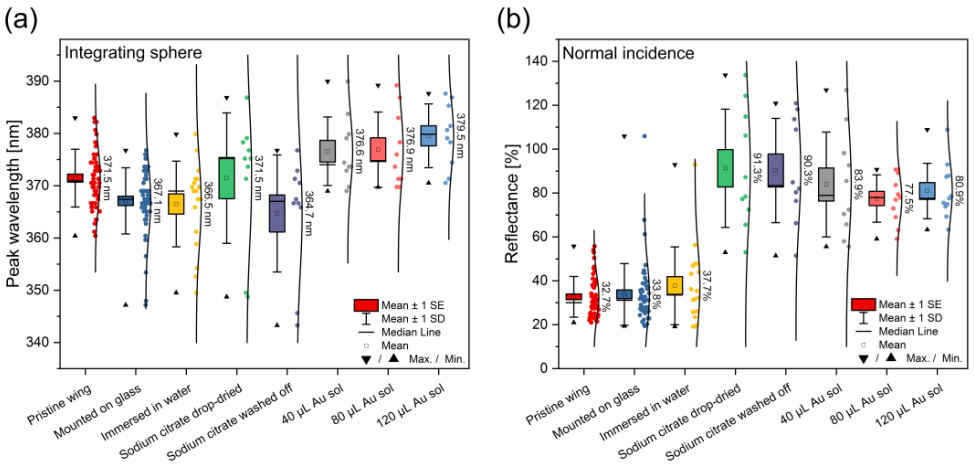

Figure 6. Statistical presentation of the changes in optical properties of male *Polyommatus icarus* wings mounted on glass substrate by PLA. (**a**) Integrating sphere measurement of the spectral position of the blue reflectance maximum after the different treatments of the wings; (**b**) normal incidence measurement of the amplitude of the blue reflectance maximum after the different treatments of the wings.

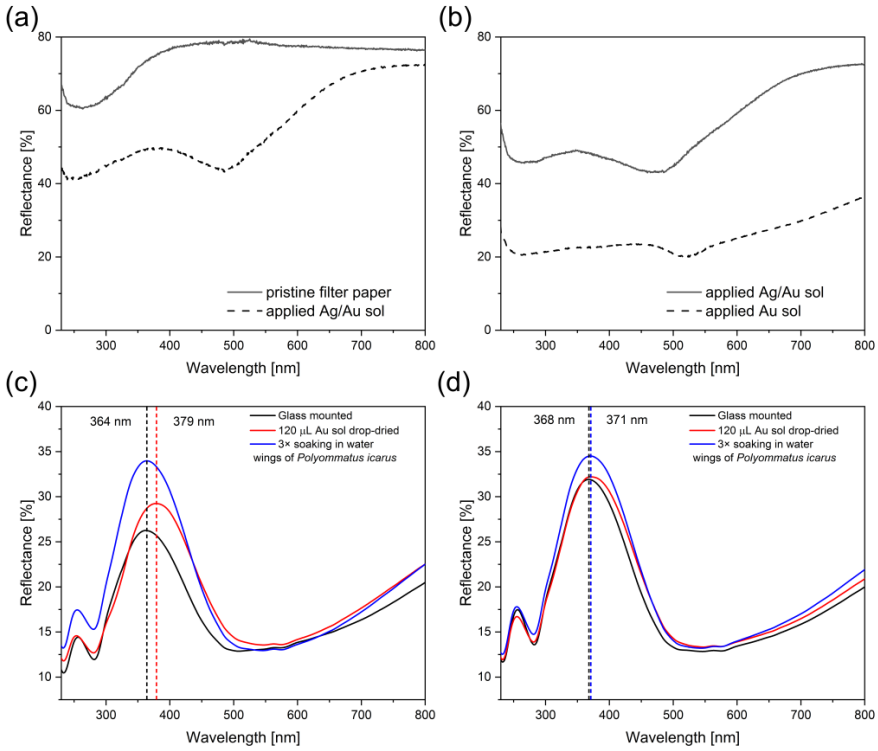

Figure 7. Reflectance measured with the integrating sphere of Au and Ag/Au NPs loaded filter papers and on blue butterfly wings of male *Polyommatus icarus* butterflies. (**a**) Pristine filter paper and Ag/Au NPs applied on the filter paper; (**b**) comparison of the reflectance of Au and Ag/Au NPs on the same type of filter paper; (**c**) butterfly wing mounted on glass substrate using PLA (black curve), after water soaking and drying followed by the application of 120 µL of Au NP sol and drying (red curve), after three cycles of soaking in deionized water (blue curve); (**d**) butterfly wing mounted on glass substrate using PLA (black curve), after water soaking and drying followed the application of 120 µL of Ag/Au NP sol and drying (red curve), after three cycles of soaking in deionized water (blue curve).

In Figure 7c,d, the reflectance of the butterfly wings pretreated by immersing in water is shown after the application of 120 µL sodium citrate-based Au and Ag/Au sols. The Ag/Au sol produced less redshift of the reflectance maximum. For both the Au and the Ag/Au sols, after three cycles of washing, the original position of the reflectance maximum was recovered, and a moderate increase in the amplitude of the reflectance maximum was observed.

The significant difference seen in Figure 3a,b between the reflectance values measured in normal incidence and with the integrating sphere for the same wings after the application of the Au NP sol, and the doubling of the reflectance intensity measured in normal incidence seen in the statistical data of Figure 6b, made it necessary to investigate the possible causes of these changes. Single scale measurements were carried out using a microspectrometer on five scales detached from a wing that was subjected only to water immersion for 8 h and drying overnight. Five scales were detached from a wing on which 120 µL of sodium citrate solution were drop-dried. The next day, the citrate-treated wing was immersed for 8 h in deionized water, dried overnight, and scales were detached for microscopic examination and spectral measurements. The micrographs of typical scales and the averaged spectra over five scales are shown in Figure 8. The sharp drop of the reflectance at about 370 nm is because the limited transmittance of the optical elements under a standard optical microscope distorts the measurements in the UV range. However, the distortion is identical for the two samples, so the differences between the samples could be effectively revealed if there were a difference, which clearly is not the case.

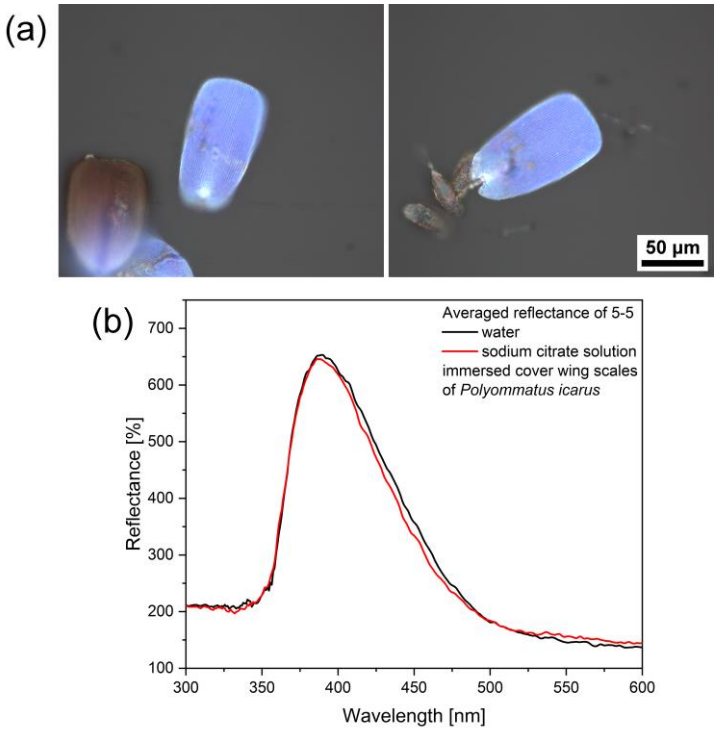

Figure 8. (**a**) Microphotographs of the single scales removed from the only water-soaked wing (left) and from the wing subjected to sodium citrate treatment (right); (**b**) comparison of the averaged reflectance curve for the two different kinds of scales. Note the sharp cutoff below 370 nm due to the glass optics of the microscope.

To make sure that neither water, nor the solution of sodium citrate affects the crystalline structure of the chitin, X-ray diffraction (XRD) measurements were performed on chitin powder in an as-received state after 6 h stirring in deionized water and drying and after 6 h stirring in the sodium citrate solution and drying. The X-ray diffractograms of the samples (Figure S7) are rather similar to literature results typical for chitin [35,36]. The XRD data did not reveal any treatment-induced modification in the crystalline structure of the chitin.

The next possibility to be investigated is the change in the angle of the scales with respect to the wing membrane. This was conducted using an optical microscope with focus stacking mode and with a calibrated stage, under which the height of the sharp image with respect to the sample plane can be precisely quantified. The results are shown in Figure 9.

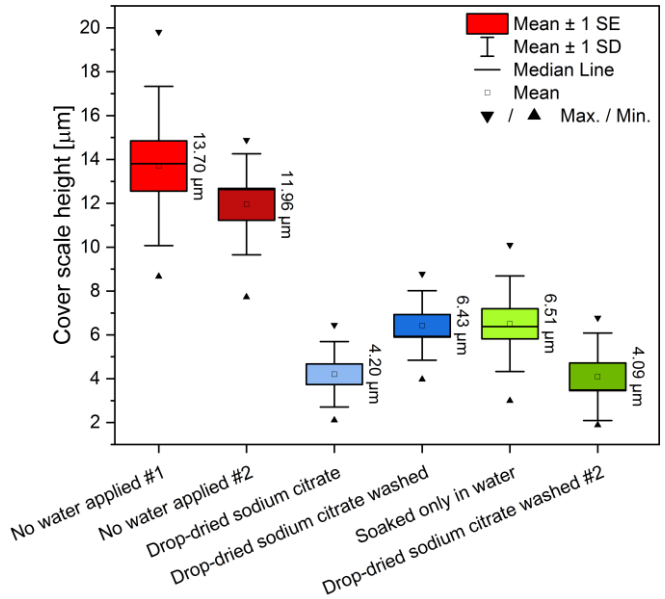

Figure 9. Height of the cover scales with respect to the wing plane as measured by a focus stacking microscope. After the citrate treatment, the height of the terminal region of the cover scales is reduced to about half of the pristine value. This indicates that the scales are flattened towards the wing membrane after the sodium citrate treatment.

As one may observe from Figure 6b, treatment with the sodium citrate solution increased the range of scattering for the amplitude of reflectance maxima from 20–60% of the wings glued onto the glass substrate to 45–135%. Therefore, it is best to compare the modifications of the same wing after the different treatments. In Figure 10, the spectra of the wing "drop-dried sodium citrate" (from Figure 9) are shown as measured by integrating sphere and under normal incidence. The wing was measured in the following conditions: (i) mounted on the glass substrate; (ii) after the application of 120 µL of sodium citrate solution and drying; (iii) first immersion in deionized water for 8 h and drying overnight; (iv) second immersion in deionized water for 8 h and drying overnight; (v) third immersion in deionized water for 8 h and drying overnight. One may observe that the integrating sphere measurement does not show a shift in the position of the reflectance maximum but shows a moderate increase of the amplitude from 25% to 40%. It has to be emphasized here that when applying a solution containing only sodium citrate on the butterfly wing, no redshift is observed in the spectral position of the reflectance maximum.

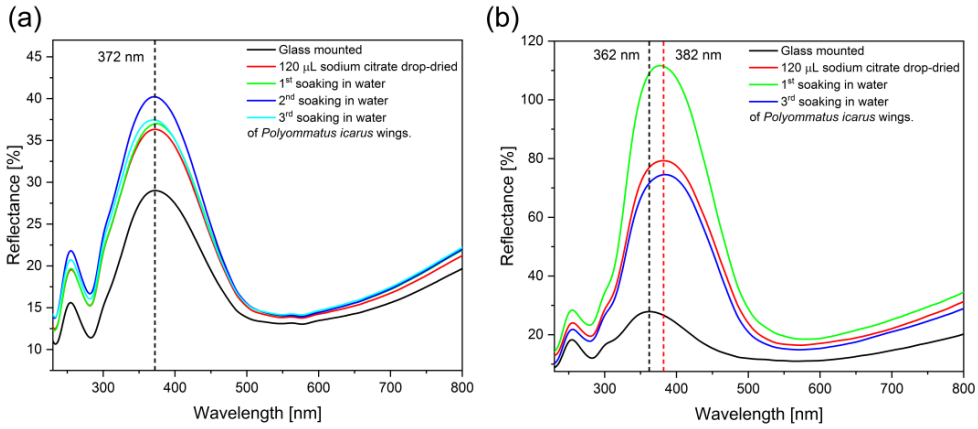

Figure 10. Spectral "history" of sample 'drop-dried sodium citrate' from Figure 9 after the application of 120 μL of sodium citrate solution and after several steps of soaking for 8 h in deionized water. Each soaking step was followed by overnight drying before re-measuring the sample. Spectra were recorded with the integrating sphere and at normal incidence for panels (**a**) and (**b**), respectively.

On the same wing, when measured in normal incidence, a redshift of 20 nm is found. This redshift is persistent; not even three steps of immersion in deionized water can eliminate it. The amplitude of the reflectance maximum increases from 20% to 80% when the sodium citrate is drop-dried, then increases to 110% after the first immersion cycle. Finally, it stabilizes at 75% after the third immersion cycle.

4. Discussion

As already outlined in the Introduction, the expected effects can be grouped as follows: (i) water-related effects; (ii) sodium citrate solution-related effects; and (iii) the effects of plasmonic metallic NPs. We will follow this order in discussing the measured effects.

4.1. Water-Related Effects

As shown in Figures 1 and 2, if no special treatment is carried out to facilitate water penetration into the chitin-based nanoarchitecture generating the color of structurally colored cover scales of the wings, the color is preserved even after 6 days of immersion in deionized water. Only a slight redshift of 18 nm is observed (Figure 2), which is eliminated during the first hour of drying. This treatment is different from the softening of butterflies used when setting the insects on a spreading board for obtaining the usual (not natural) wing positions seen in collections. During this treatment, the butterflies are exposed to saturated water vapors in closed containers for several days. The daily temperature fluctuations produce the condensation of water vapors in the nanoarchitecture in a similar way, as reported in the case of butterfly wings used as selective chemical sensors [37–41]. Liquid water cannot penetrate the nanoarchitecture because the butterfly wing is superhydrophobic [33]. Figure 6a,b also shows that when multiple samples are evaluated statistically, the water immersion does not produce significant changes if the samples are measured after complete drying. A change is observed when a drop of ethanol is used prior to the immersion in water to facilitate the penetration of the water in the nanovoids of the wing scales (soaking). As seen in Figure 9, after drying, the position of the scales with respect to the wing plane is modified.

4.2. Sodium Citrate Solution Related Effects

When drop-drying sodium citrate solution on the wings, irrespective of whether the citrate solution was produced by the centrifugation of Au NP sol and using the clear supernatant, or was produced by dissolving sodium citrate in water, if ethanol was used to facilitate the penetration of the aqueous solution in the nanoarchitecture, the following modifications were induced: a small and reversible redshift of the reflectance maximum when measured with an integrating sphere (Figure 6a) and a significant increase in the normal incidence reflectance (Figure 6b). The effect on the very same wing of the different subsequent treatments is exemplified in Figure 10. It is not surprising that the modification of the angle of the scales with respect to the wing plane influences the normal incidence reflectance. However, the magnitude of the effect is quite remarkable. The cover scales are fixed to the wing membrane with a so-called pedicel, fixed in the scale socket of the wing membrane (Figure S5). In fact, the pedicel is a hollow tube through which the scale-producing cell is connected to its nucleus-containing part located in the wing membrane [42]. This pedicel provides a flexible connection of the cover scale to the wing membrane at an angle of approximately 20°. Due to the surface tension of water, or water-based sodium citrate solution, when water could penetrate the nanoarchitectures of the wing surface, during subsequent drying, the wing scales will be flattened towards each other and the wing membrane. They will keep this position even in a completely dried state, such as how set butterflies in collections preserve the unnatural wing position in which their wings were arranged during setting. The reduction of the angle of the cover scales with respect to the wing membrane (Figure 9) is responsible for the increased reflectance under normal incidence as the incoming light will fall on the scale under an angle closer to the scale normal. The reflectance measurements carried out with an integrating sphere are less sensitive to this effect of scale angle modification because, in these conditions, all incidence angles of the upper hemisphere are equally taken into account (for the difference between normal incidence and integrating sphere measurements of butterfly wing with structural coloration, see for example Figure 4 of [43].

From Figures 6 and 10, one can observe that the sodium citrate solution alone has no or only a very moderate effect on the spectral position of the reflectance maximum measured with an integrating sphere, but produces a significant increase in the amplitude of the reflectance maximum, when measured under normal incidence. The statistical evaluation of the immersion in deionized water (Figure 6) shows that the modification of the spectral position, if any, is eliminated, while the increase in the normal incidence reflectance is conserved. The repeated cycles of immersion for 8 h in deionized water, followed by overnight drying and measurement the next day carried out on the same sample (Figure 10), show similar results. Figure 9 also show that both for soaking in pure water and in water-based sodium citrate solution, the modification of scale position is similar.

One may conclude that the main effect of both water and water-based sodium citrate solution is the remnant modification of the angle between the cover scale and the wing membrane.

4.3. Metallic Nanoparticle-Related Effects

The extinction of the metallic NPs was measured in the sodium citrate solution in which they were produced. The results are shown in Figures S2 and S3. Both the Au and the Ag/Au NPs exhibited the expected extinction determined by their composition and size. As seen in Figure S3, the absorbance maximum of the Ag/Au NPs (metal ratio 1:1) is at 454 nm, in good agreement with literature data [44].

The metallic NPs were loaded once onto filter paper and in several experiments into the photonic nanoarchitectures of the cover scales on butterfly wings. The filter paper was used as a comparison sample, which is chemically close to chitin, has a porous structure similar to butterfly wings, and behaves as a Lambertian reflector [45]. The basic constituent of paper, cellulose, is also a transparent polysaccharide like chitin and has a chemical

composition very similar to that of chitin [34]. On the metallic nanoparticles loaded filter paper samples, the general decrease of the reflectance and appearance of the characteristic extinction bands for the Au and Ag/Au sols were observed. In Figure 7a, the reflectance of the Ag/Au sol-loaded filter paper is compared to the reflectance of the pristine filter paper. One may observe that the relatively high (75%) reflectance of the filter paper starts to decrease from 400 nm towards the UV. The Ag/Au NP-loaded filter paper behaves in the same way in this spectral range. The difference between the pristine paper and the Ag/Au NP-loaded paper is clearly present between 700 and 400 nm. A slight redshift of the absorption on the Ag/Au NPs and a broadening of the absorption band can be observed if comparing Figure 7a with Figure S3. These effects may be associated with the clustering of the NPs.

In Figure 7b, the reflectance spectra of the filter papers loaded with Ag/Au and Au NPs are compared. In agreement with the spectral position of the extinction spectra, the reflectance minimum of the Au NP loaded filter paper is on the red side of the reflectance minimum of the Ag/Au NP loaded paper. None of the samples exhibit features which may be associated with the sodium citrate present in the samples.

When the same NPs were applied on butterfly wings, they did not produce visible absorption bands in the spectral position where their absorption band was observed on the filter paper but instead produced the redshift of the reflectance peaks of the photonic nanoarchitecture, Figure 7c,d. This indicates that the butterfly wing scales, with the NPs, integrated into the photonic nanoarchitecture, as seen in Figure 5, behave like a complex nanocomposite which inherits its properties from both the chitin-based photonic nanoarchitecture and from the metallic NPs. As the composite is made up dominantly of the chitin-based biologic photonic nanoarchitecture, its properties are primarily determined by photonic nanoarchitectures of the butterfly wing scales. The presence of the metallic NPs is not manifested independently, such as in the case of the paper samples, when the characteristic absorption bands of the plasmonic NPs were observed. Instead, combined properties are found which are different from both those of the pristine biologic photonic nanoarchitecture and from those of the plasmonic metallic NPs. This type of behavior is known for hybrid photonic crystals, for example, when depositing a continuous metallic layer with a thickness in the nanometer range on dielectric nanospheres [46]. Photonic stop-band tuning by the deposition of thin metallic layers on opals and invers opals were reported recently [47]. A similar combination of photonic and plasmonic effects was reported after Au NP infiltration for thin films of photonic crystals with inverse opal structure prepared by photocurable resin polymerization on opal templates [48]. A further possibility for tuning the chemical effects of such hybrid photonic nanoarchitectures may be offered by the phenomenon known in the literature as strong coupling [13,49–51]. In the strong coupling regime, hybrid light-matter states are formed. The hybridization is not limited to electronic transitions; it can be applied, for instance, to vibrational transitions to selectively perturb a given bond, opening new possibilities to change the chemical reactivity landscape and to use it as a tool in molecular science and spectroscopy [13]. This "wedding" of electromagnetic radiation and matter offers further advantages as compared with the simple use of porous polymeric substrates only for supporting the NPs [8]. For example, the strong coupling in a nanocavity was reported for methylene-blue molecules, at room temperature and in ambient conditions [52]. The plasmonic NPs located inside the nanocavities of the photonic nanoarchitecture, which is not allowing the propagation of electromagnetic radiation within a certain wavelength range, may exhibit resonant absorption in the vicinity of the stop band as reported for Au NPs in inverse opal photonic crystals [49]. On the other hand, under ambient conditions, the effect of the photonic stop band only, in the absence of plasmonic NPs, on the amplitude of spontaneous Raman scattering peaks for inverse opal samples was recently reported [53]. An enhancement of the Raman spectra due to the coincidence of the stop band center with the laser wavelength was shown; the enhancement factor was estimated to be more than 50.

Similar to the position of the absorption bands of the alloyed Ag/Au and Au NPs (Figures S2, S3 and 7b), the effect of the two different kinds of NPs on the optical properties of the butterfly wing is different. The Ag/Au NPs produce a smaller redshift as compared with the Au NPs (Figure 7c,d). This may be associated with their absorption band centered at 454 nm being closer to the reflectance peak of the pristine photonic nanoarchitecture at 365 nm, Figure S4. For both kinds of metallic NPs, the blue edge of the reflectance peak of the photonic nanoarchitecture is not altered; only the red edge is modified. The magnitude of the redshift is dependent on the concentration of the metallic NPs, as seen in Figure 4. However, one has to be careful to avoid the coalescence of the NPs, because this will destroy the photonic band gap and will yield behavior resembling that of bulk gold (Figure S6).

After repeatedly washing the wings on which Au NPs were deposited with deionized water, the redshift of the peaks was eliminated (Figure 7c,d), and only the somewhat increased reflectance, which was already observed for water and water-based sodium citrate treatment, was observed. This shows that the redshift was caused by the presence of the metallic NPs and indicates that the surface chemistry of the chitin substrate must be modified to provide a stronger chemical fixation of the NPs. This could be achieved by physical means, such as short time oxygen plasma treatment or conformal atomic layer deposition [54] of suitable chemical compounds, such as ZnO or TiO_2, which could contribute to enhancing the photocatalytic effect too [55,56]. Recently, an enhanced photocatalytic effect was reported on butterfly wings possessing structural color and conformally coated by ZnO [57].

5. Conclusions

The investigation of the effects of drop-dried sodium citrate-based Au and alloyed Ag/Au NP sols on the optical properties of the wings of male *Polyommatus icarus* butterflies possessing blue structural color on their dorsal wings showed that the effects of water, sodium citrate, and plasmonic metallic NPs could be separated.

The effects produced by pure deionized water depend on the use of ethanol to facilitate the penetration of liquid water inside the photonic nanoarchitecture: if no ethanol is used, liquid water cannot penetrate into the superhydrophobic photonic nanoarchitecture and even after several days of water immersion the structural color is preserved with a minor redshift of the reflectance maximum. This redshift is eliminated in the first hour of drying in ambient air. If ethanol facilitates the penetration of deionized water inside the photonic nanoarchitecture, the major effect measured after drying is the increase of normal incidence reflectance caused by the flattening of the wing scales towards the wing membrane. This effect is persistent.

When drop-drying sodium citrate solutions on the wings in all experiments, ethanol was used to facilitate the penetration of the sol inside the photonic nanoarchitecture. No or only minor spectral shift and amplitude increase were observed for the reflectance maximum measured with the integrating sphere, but a significant increase was found in the amplitude of the normal incidence reflectance. After washing with deionized water, the spectral shift measured with the integrating sphere, if present, was eliminated, but the increased amplitude of the normal incidence reflectance peak was maintained. This, as in the case of pure deionized water, is caused by the alteration of scale position with respect to the wing membrane.

The Au and Ag/Au NPs caused the redshift of the reflectance maximum measured with an integrating sphere. The magnitude of the redshift was higher for the Au NPs, which have the characteristic absorption band at a longer wavelength compared to the absorption band of the alloyed Ag/Au NPs. The redshift increased with the increasing concentration of the metallic NPs used, but the coalescence of the NPs must be avoided as this can replace the photonic properties by bulk metallic behavior. On filter paper-based comparison samples, with a very close chemical composition but without photonic nanoarchitecture, only the characteristic absorption bands of the NPs could be measured. These results are interpreted as the presence of hybridization between the photonic nanoarchitecture and

the metallic NPs with plasmonic properties. When the NPs were removed by repeated washing, the redshift was eliminated.

Supplementary Materials: The following supporting information can be downloaded at: https://www.mdpi.com/article/10.3390/photonics9080553/s1, Figure S1: Custom-made apparatus (a) with feeding *Polyommatus icarus* specimens (b) in which the vegetation and the climate of the habitat needed by the butterflies can be replicated; Figure S2: Absorbance of the Au nanoparticles in sodium citrate solution; Figure S3: Absorbance of the Ag/Au nanoparticles in sodium citrate solution; Figure S4: Reflectance spectra measured with an integrating sphere of the pristine wings on which later different amounts of Au sols were applied in Figure 4; Figure S5: SEM images of (a) a pedicel of a cover scale and (b) a socket which connects it to the wing membrane; Figure S6: *Polyommatus icarus* wing treated with Au sol. (a) Brown region can be observed where the coalescence of the Au nanoparticle occurred. (b) Normal incidence reflectance of the blue region of the wing and of the brown region of the same wing, where the coalescence occurred; Figure S7: X-ray diffractograms of the chitin in an as-received state (Pristine); after 6 h continuous stirring in deionized water (Water); and in sodium citrate solution (Citrate). One cannot observe any significant alteration in the XRD plots.

Author Contributions: Conceptualization, L.P.B.; methodology, D.Z., A.D., and L.P.B.; investigation, K.K., G.P., and Z.E.H.; resources, A.D.; data curation, K.K.; writing—original draft preparation, L.P.B.; writing—review and editing, K.K., G.P., Z.E.H., D.Z., and A.D.; visualization, K.K. and G.P.; supervision, L.P.B.; project administration, K.K.; funding acquisition, L.P.B. and A.D. All authors have read and agreed to the published version of the manuscript.

Funding: Project no. TKP2021-NKTA-05 has been implemented with the support provided by the Ministry of Innovation and Technology of Hungary from the National Research, Development and Innovation Fund, financed under the TKP2021 funding scheme. Funding from the National Research, Development and Innovation Office—NKFIH FK128327 is acknowledged.

Institutional Review Board Statement: Not applicable.

Informed Consent Statement: Not applicable.

Data Availability Statement: The data that support the findings of this study are available from the corresponding author upon reasonable request.

Acknowledgments: The authors wish to thank Andrea Beck of the Institute for Energy Security and Environmental Safety, Surface Chemistry and Catalysis Department, Centre for Energy Research, Budapest, Hungary, for preparing and characterizing the Ag/Au nanoparticle sol. This research was supported by the János Bolyai Research Scholarship of the Hungarian Academy of Sciences (G.P.).

Conflicts of Interest: The authors declare no conflict of interest.

References

1. Zhou, L.; Swearer, D.F.; Zhang, C.; Robatjazi, H.; Zhao, H.; Henderson, L.; Dong, L.; Christopher, P.; Carter, E.A.; Nordlander, P.; et al. Quantifying hot carrier and thermal contributions in plasmonic photocatalysis. *Science* **2018**, *362*, 69–72. [CrossRef] [PubMed]
2. Aslam, U.; Rao, V.G.; Chavez, S.; Linic, S. Catalytic conversion of solar to chemical energy on plasmonic metal nanostructures. *Nat. Catal.* **2018**, *1*, 656–665. [CrossRef]
3. Zhao, J.; Nguyen, S.C.; Ye, R.; Ye, B.; Weller, H.; Somorjai, G.A.; Alivisatos, A.P.; Toste, F.D. A Comparison of Photocatalytic Activities of Gold Nanoparticles Following Plasmonic and Interband Excitation and a Strategy for Harnessing Interband Hot Carriers for Solution Phase Photocatalysis. *ACS Cent. Sci.* **2017**, *3*, 482–488. [CrossRef] [PubMed]
4. Diallo, M.; Duncan, J.; Savage, N.; Street, A.; Sustich, R. *Nanotechnology Applications for Clean Water: Solutions for Improving Water Quality*, 2nd ed.; William Andrew: Waltham, MA, USA, 2014.
5. Ezeuko, A.S.; Ojemaye, M.O.; Okoh, O.O.; Okoh, A.I. Potentials of metallic nanoparticles for the removal of antibiotic resistant bacteria and antibiotic resistance genes from wastewater: A critical review. *J. Water Process Eng.* **2021**, *41*, 102041. [CrossRef]
6. Chauhan, G.; González-González, R.B.; Iqbal, H.M.N. Bioremediation and decontamination potentials of metallic nanoparticles loaded nanohybrid matrices—A review. *Environ. Res.* **2022**, *204*, 112407. [CrossRef]
7. Gellé, A.; Jin, T.; de la Garza, L.; Price, G.D.; Besteiro, L.V.; Moores, A. Applications of Plasmon-Enhanced Nanocatalysis to Organic Transformations. *Chem. Rev.* **2020**, *120*, 986–1041. [CrossRef]
8. Poupart, R.; Grande, D.; Carbonnier, B.; Le Droumaguet, B. Porous polymers and metallic nanoparticles: A hybrid wedding as a robust method toward efficient supported catalytic systems. *Prog. Polym. Sci.* **2019**, *96*, 21–42. [CrossRef]

9. Raja-Mogan, T.; Ohtani, B.; Kowalska, E. Photonic Crystals for Plasmonic Photocatalysis. *Catalysts* **2020**, *10*, 827. [CrossRef]
10. Qiu, Y.; Yang, Y.; Valenzuela, C.; Zhang, X.; Yang, M.; Xue, P.; Ma, J.; Liu, Z.; Wang, L.; Feng, W. Near-Infrared Light-Driven Three-Dimensional Soft Photonic Crystals Loaded with Upconversion Nanoparticles. *Adv. Opt. Mater.* **2022**, *10*, 2102475. [CrossRef]
11. Liu, J.; Wu, M.; Van der Schueren, B.; Deparis, O.; Ye, J.; Ozin, G.A.; Hasan, T.; Su, B.L. Slow Photons for Photocatalysis and Photovoltaics. *Adv. Mater.* **2017**, *29*, 1605349. [CrossRef]
12. Thomas, A.; Lethuillier-Karl, L.; Nagarajan, K.; Vergauwe, R.M.A.; George, J.; Chervy, T.; Shalabney, A.; Devaux, E.; Genet, C.; Moran, J.; et al. Tilting a ground-state reactivity landscape by vibrational strong coupling. *Science* **2019**, *363*, 615–619. [CrossRef] [PubMed]
13. Ebbesen, T.W. Hybrid Light–Matter States in a Molecular and Material Science Perspective. *Acc. Chem. Res.* **2016**, *49*, 2403–2412. [CrossRef] [PubMed]
14. Cai, Z.; Li, Z.; Ravaine, S.; He, M.; Song, Y.; Yin, Y.; Zheng, H.; Teng, J.; Zhang, A. From colloidal particles to photonic crystals: Advances in self-assembly and their emerging applications. *Chem. Soc. Rev.* **2021**, *50*, 5898–5951. [CrossRef] [PubMed]
15. Biró, L.P.; Vigneron, J.P. Photonic nanoarchitectures in butterflies and beetles: Valuable sources for bioinspiration. *Laser Photonics Rev.* **2011**, *5*, 27–51. [CrossRef]
16. Bálint, Z.; Kertész, K.; Piszter, G.; Vértesy, Z.; Biró, L.P. The well-tuned blues: The role of structural colours as optical signals in the species recognition of a local butterfly fauna (Lepidoptera: Lycaenidae: Polyommatinae). *J. R. Soc. Interface* **2012**, *9*, 1745–1756. [CrossRef] [PubMed]
17. Stavenga, D.G. Thin Film and Multilayer Optics Cause Structural Colors of Many Insects and Birds. *Mater. Today Proc.* **2014**, *1*, 109–121. [CrossRef]
18. Ingram, A.L.; Parker, A.R. A review of the diversity and evolution of photonic structures in butterflies, incorporating the work of John Huxley (The Natural History Museum, London from 1961 to 1990). *Philos. Trans. R. Soc. Lond. Ser. B* **2008**, *363*, 2465–2480. [CrossRef]
19. Giraldo, M.A.; Stavenga, D.G. Brilliant iridescence of Morpho butterfly wing scales is due to both a thin film lower lamina and a multilayered upper lamina. *J. Comp. Physiol. A* **2016**, *202*, 381–388. [CrossRef]
20. Kinoshita, S.; Yoshioka, S. Structural colors in nature: The role of regularity and irregularity in the structure. *Chemphyschem* **2005**, *6*, 1442–1459. [CrossRef]
21. Wilts, B.D.; Giraldo, M.A.; Stavenga, D.G. Unique wing scale photonics of male Rajah Brooke's birdwing butterflies. *Front. Zool.* **2016**, *13*, 36. [CrossRef]
22. Kertész, K.; Piszter, G.; Bálint, Z.; Biró, L.P. Biogeographical patterns in the structural blue of male *Polyommatus icarus* butterflies. *Sci. Rep.* **2019**, *9*, 2338. [CrossRef] [PubMed]
23. Piszter, G.; Kertész, K.; Bálint, Z.; Biró, L.P. Variability of the Structural Coloration in Two Butterfly Species with Different Prezygotic Mating Strategies. *PLoS ONE* **2016**, *11*, e0165857. [CrossRef] [PubMed]
24. Piszter, G.; Kertész, K.; Sramkó, G.; Krízsik, V.; Bálint, Z.; Biró, L.P. Concordance of the spectral properties of dorsal wing scales with the phylogeographic structure of European male *Polyommatus icarus* butterflies. *Sci. Rep.* **2021**, *11*, 16498. [CrossRef] [PubMed]
25. Liz-Marzán, L.M. Nanometals: Formation and color. *Mater. Today* **2004**, *7*, 26–31. [CrossRef]
26. Zámbó, D.; Radnóczi, G.Z.; Deák, A. Preparation of Compact Nanoparticle Clusters from Polyethylene Glycol-Coated Gold Nanoparticles by Fine-Tuning Colloidal Interactions. *Langmuir* **2015**, *31*, 2662–2668. [CrossRef]
27. Ismail, A.M.; Csapó, E.; Janáky, C. Correlation between the work function of Au–Ag nanoalloys and their electrocatalytic activity in carbon dioxide reduction. *Electrochim. Acta* **2019**, *313*, 171–178. [CrossRef]
28. The Global Silk Industry: Perception of European Operators toward Thai Natural & Organic Silk Fabric and Final Products. Available online: https://www.fibre2fashion.com/industry-article/6015/the-global-silk-industry (accessed on 17 June 2022).
29. Czaplicki, Z.; Gliścińska, E.; Machnowski, W. Natural Silk—An Unusual Fibre: Origin, Processing and World Production. *Fibres Text. East. Eur.* **2021**, *29*, 22–28. [CrossRef]
30. Piszter, G.; Kertész, K.; Horváth, Z.E.; Bálint, Z.; Biró, L.P. Reproducible phenotype alteration due to prolonged cooling of the pupae of *Polyommatus icarus* butterflies. *PLoS ONE* **2019**, *14*, e0225388. [CrossRef]
31. Cooper Stevenson, P.A. Study of the Nucleation and Growth Processes in the Synthesis of Colloidal Gold. *Discuss. Faraday Soc.* **1951**, *11*, 55–75. [CrossRef]
32. Csapó, E.; Oszkó, A.; Varga, E.; Juhász, Á.; Buzás, N.; Kőrösi, L.; Majzik, A.; Dékány, I. Synthesis and characterization of Ag/Au alloy and core(Ag)–shell(Au) nanoparticles. *Colloids Surf. A* **2012**, *415*, 281–287. [CrossRef]
33. Han, Z.; Fu, J.; Wang, Z.; Wang, Y.; Li, B.; Mu, Z.; Zhang, J.; Niu, S. Long-term durability of superhydrophobic properties of butterfly wing scales after continuous contact with water. *Colloids Surf. A* **2017**, *518*, 139–144. [CrossRef]
34. Kostag, M.; El Seoud, O.A. Sustainable biomaterials based on cellulose, chitin and chitosan composites—A review. *Carbohydr. Polym. Technol. Appl.* **2021**, *2*, 100079. [CrossRef]
35. Minke, R.; Blackwell, J. The structure of a-chitin. *J. Mol. Biol.* **1978**, *20*, 167–181. [CrossRef]
36. Zhong, T.H.; Wolcott, M.P.; Liu, H.; Glandon, N.; Wang, J.W. The influence of pre-fibrillation via planetary ball milling on the extraction and properties of chitin nanofibers. *Cellulose* **2020**, *27*, 6205–6216. [CrossRef]

37. Piszter, G.; Kertész, K.; Vértesy, Z.; Bálint, Z.; Biró, L.P. Substance specific chemical sensing with pristine and modified photonic nanoarchitectures occurring in blue butterfly wing scales. *Opt. Express* **2014**, *22*, 22649. [CrossRef]
38. Piszter, G.; Kertész, K.; Bálint, Z.; Biró, L.P. Pretreated butterfly wings for tuning the selective vapor sensing. *Sensors* **2016**, *16*, 1446. [CrossRef] [PubMed]
39. Kertész, K.; Piszter, G.; Bálint, Z.; Biró, L.P. Optical Vapor Sensing on Single Wing Scales and on Whole Wings of the *Albulina metallica* Butterfly. *Sensors* **2018**, *18*, 4282. [CrossRef] [PubMed]
40. Piszter, G.; Kertész, K.; Bálint, Z.; Biró, L.P. Optical detection of vapor mixtures using structurally colored butterfly and moth wings. *Sensors* **2019**, *19*, 3058. [CrossRef]
41. Piszter, G.; Kertész, K.; Bálint, Z.; Biró, L.P. Stability and Selective Vapor Sensing of Structurally Colored Lepidopteran Wings Under Humid Conditions. *Sensors* **2020**, *20*, 3258. [CrossRef]
42. Greenstein, M.E. The ultrastructure of developing wings in the giant silkmoth, *Hyalophora cecropia*. II. Scale-forming and socket-forming cells. *J. Morphol.* **1972**, *136*, 23–51. [CrossRef]
43. Kertész, K.; Bálint, Z.; Piszter, G.; Horváth, Z.E.; Biró, L.P. Multi-instrumental techniques for evaluating butterfly structural colors: A case study on *Polyommatus bellargus* (Rottemburg, 1775) (Lepidoptera: Lycaenidae: Polyommatinae). *Arthropod Struct. Dev.* **2021**, *61*, 101010. [CrossRef] [PubMed]
44. Sun, Y.; Xia, Y. Gold and silver nanoparticles: A class of chromophores with colors tunable in the range from 400 to 750 nm. *Analyst* **2003**, *128*, 686. [CrossRef] [PubMed]
45. Koppal, S.J. Lambertian Reflectance. In *Computer Vision*; Springer: Boston, MA, USA, 2014; pp. 441–443. [CrossRef]
46. Romanov, S.G.; Korovin, A.V.; Regensburger, A.; Peschel, U. Hybrid Colloidal Plasmonic-Photonic Crystals. *Adv. Mater.* **2011**, *23*, 2515–2533. [CrossRef] [PubMed]
47. Lonergan, A.; Murphy, B.; O'Dwyer, C. Photonic Stopband Tuning in Metallo-Dielectric Photonic Crystals. *ECS J. Solid State Sci. Technol.* **2021**, *10*, 085001. [CrossRef]
48. Klimonsky, S.; Baranchikov, A.; Lad, V.N.; Eremina, E.; Garshev, A.; Kuznetsov, A.; Jalolov, F.; Demidovich, P. Photonic and plasmonic effects in inverse opal films with Au nanoparticles. *Photonics Nanostruct. Fundam. Appl.* **2021**, *43*, 100899. [CrossRef]
49. Kolaric, B.; Maes, B.; Clays, K.; Durt, T.; Caudano, Y. Strong Light—Matter Coupling as a New Tool for Molecular and Material Engineering: Quantum Approach. *Adv. Quantum Technol.* **2018**, *1*, 1800001. [CrossRef]
50. Dovzhenko, D.S.; Ryabchuk, S.V.; Rakovich, Y.P.; Nabiev, I.R. Light–matter interaction in the strong coupling regime: Configurations, conditions, and applications. *Nanoscale* **2018**, *10*, 3589–3605. [CrossRef]
51. Ameling, R.; Giessen, H. Microcavity plasmonics: Strong coupling of photonic cavities and plasmons. *Laser Photonics Rev.* **2013**, *7*, 141–169. [CrossRef]
52. Chikkaraddy, R.; de Nijs, B.; Benz, F.; Barrow, S.J.; Scherman, O.A.; Rosta, E.; Demetriadou, A.; Fox, P.; Hess, O.; Baumberg, J.J. Single-molecule strong coupling at room temperature in plasmonic nanocavities. *Nature* **2016**, *535*, 127–130. [CrossRef]
53. Ashurov, M.; Baranchikov, A.; Klimonsky, S. Photonic crystal enhancement of Raman scattering. *Phys. Chem. Chem. Phys.* **2020**, *22*, 9630–9636. [CrossRef]
54. Kertész, K.; Baji, Z.; Deák, A.; Piszter, G.; Rázga, Z.; Bálint, Z.; Biró, L.P. Additive and subtractive modification of butterfly wing structural colors. *Colloid Interface Sci. Commun.* **2021**, *40*, 100346. [CrossRef]
55. Likodimos, V. Photonic crystal-assisted visible light activated TiO_2 photocatalysis. *Appl. Catal. B* **2018**, *230*, 269–303. [CrossRef]
56. Zheng, X.; Zhang, Z.; Meng, S.; Wang, Y.; Li, D. Regulating charge transfer over 3D Au/ZnO hybrid inverse opal toward efficiently photocatalytic degradation of bisphenol A and photoelectrochemical water splitting. *Chem. Eng. J.* **2020**, *393*, 124676. [CrossRef]
57. Piszter, G.; Kertész, K.; Nagy, G.; Baji, Z.; Horváth, Z.E.; Bálint, Z.; Sándor Pap, J.; Biró, L.P. Spectral tuning of biotemplated ZnO photonic nanoarchitectures for photocatalytic applications. *R. Soc. Open Sci.* **2022**, *9*, 220090. [CrossRef]